

To: PE&RS Authors

From: Mike Renslow
Technical Editor

Thank you for using our online proofing process. On the pages following this letter, please find the PDF file for your paper being published in *Photogrammetric Engineering & Remote Sensing*.

Please examine this proof, make whatever corrections are necessary, and email the edited version to me (renslow76@comcast.net) as soon as possible. You may send your corrections using postal or delivery services to the address shown below.

Even though the proof is carefully studied by skilled proofreaders, an author can usually detect discrepancies which may be obscure to anyone else. This is particularly true in the case of equations and tables.

Please confine your corrections to errors in typesetting, spelling, etc., and refrain from making extensive changes or additions which are expensive to incorporate at this stage. You are allowed to make eight (8) changes to the proof; you may be charged for additional edits.

Please note that the quality of your PDF proof on the screen, particularly the illustrations, depends on your computer equipment and software.

A “PE&RS Offprint Order Form” and “Assignment of Copyright to ASPRS” form are also attached in PDF format. Offprints must be ordered at this time so that they can be printed while the Journal is being printed. Both of the completed forms are to be returned to the Production Department, ASPRS 5410 Grosvenor Lane, Suite 210, Bethesda, MD 20814-2160 preferably by email (rkelley@asprs.org).

Please Note: In the event your paper is longer than seven (7) pages, you will be charged extra page fees. These fees are \$125 for every page over seven. The “PE&RS Offprint Order Form” has a space for extra page fees to be paid. These fees must be paid prior to your paper being printed. If you have questions about the extra page fees, please refer to the Instructions for Authors.

Sincerely,

Mike Renslow
Technical Editor – PE&RS
2880 Bailey Hill Road
Eugene, OR 97405
Tele: (541) 335-1251
E-mail: renslow76@comcast.net

Registration of Optical Images with Lidar Data and Its Accuracy Assessment

Shunyi Zheng, Rongyong Huang, and Yang Zhou

Abstract

Photogrammetry and lidar are two technologies complementary for 3D reconstruction. However, the problem is that the current registration methods of optical images with lidar data cannot satisfy all the requirements for the fusion of the above two technologies, especially for close-range photogrammetry and terrestrial lidar. In this paper, we propose a novel method for registration of optical images with terrestrial lidar data, which is implemented by minimizing the distances from the photogrammetric matching points to terrestrial lidar data surface, with the collinearity equation as the basic mathematical model. One advantage of this method is that it requires no feature extraction and segmentation from the lidar data. Another advantage is that non-rigid deformation caused by lens distortion can be eliminated through the use of bundle adjustment similar to self-calibration. In addition, experiments with two different data sets show that this method cannot only eliminate the influence of certain gross errors, but also offer a high accuracy of 3 mm to ~5 mm. Therefore, the proposed registration method is proved to be more effective, accurate, and reliable.

Introduction

Laser, as one of the most important technological developments of the twentieth century, was introduced into the field of photogrammetry in the 1980s. The result is generally known as Light Detection and Ranging (lidar) technology. It has been widely researched, developed, and applied in many fields (Baltsavias, 1999), such as 3D building model reconstruction (Cheng *et al.*, 2011), three-dimensional mapping (Vosselman *et al.*, 2005), and coastal blufflines extraction (Liu *et al.*, 2009), etc. Most of the studies have shown that photogrammetry and lidar are fairly complementary, therefore, their integration can lead to more accurate and complete products and a higher automation level of processes (Ackermann, 1999; Baltsavias, 1999; Leberl *et al.*, 2010). In order to render the point cloud with texture for preservation of cultural relics, this paper focused on the registration of optical images with lidar data. Although it is mainly aimed at texturing the point cloud, the research can also be employed as the basis of the integration of photogrammetry and lidar. In other words, due to the optical image and lidar point cloud are highly complementary in physical information and geometry information, the registration result of the research can also be widely used as the basis of the applications that require the fusion of optical images and lidar data, e.g., ortho-rectification, feature extraction, recognition and orientation, and three-dimensional modeling, etc.

The complementation of photogrammetry and lidar can be fully implemented only after successful alignment or absolute orientation of the photogrammetric and lidar models relative to a common reference frame (Postolov *et al.*, 1999; Habib *et al.*, 2006). Unlike the conventional registration between 2D images, the registration of optical images with lidar data is aimed at aligning the 2D images and the 3D point cloud relative to a common reference frame. The most effective registration procedure addresses the following issues: Registration Primitives, Similarity Measure, Registration Transformation Function, and Matching Strategy (Brown, 1992; Habib *et al.*, 2005). At present, research about the registration can be divided into three categories: 2D image matching-based registration, linear and planar feature-based registration, and 3D to 3D point cloud-based registration.

In order to solve the Registration Primitives issue, 2D image matching-based registration first transforms registration of 2D images with 3D lidar data into 2D image registration, and then compares either the grayscale values of patches of the 2D images or the descriptors of the extracted feature points to find conjugate image locations. The way to realize 2D image matching-based registration is to match lidar intensity images and optical images with some common image matching methods. Ding *et al.* (2008) developed a two-step automated registration algorithm in which the correspondence between an image and the 3D model is performed with Hough transform and generalized M-estimator sample consensus. Wu *et al.* (2010) presented a novel linear registration algorithm for aerial images and lidar data, using Tilt Displacement Correction and Height Displacement Correction. Wang *et al.* (2012) also presented a study of a multisource image automatic registration system (MIARS) based on the scale-invariant feature transform (SIFT), i.e., lidar intensity images and aerial images. Similarly, Kurz *et al.* (2011) registered spectral panoramic imagery and lidar data with control point measurement and block adjustment. It is natural to attempt to solve the correspondent issues by selecting corresponding features manually or matching the lidar intensity images and the optical images with the aid of Correlation Coefficient, SIFT, and Shape context, etc. However, as shown in Figure 1, on one hand, the manual method for the data sets is slow and labor-intensive, with limited accuracy and applicability in real tasks. On the other hand, the differences between visible and infrared spectrum always lead to difficulties in feature point extracting and image matching.

School of Remote Sensing and Information Engineering,
Wuhan University, No. 129 Luoyu Road, Wuhan 430079,
PR China (syzheng@263.net).

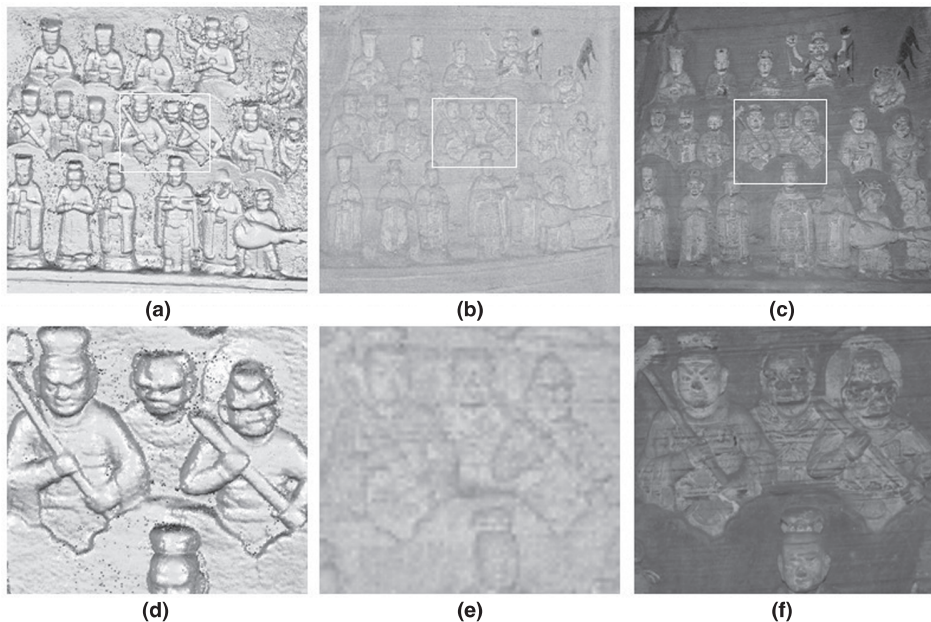


Figure 1. Lidar Data and Corresponding Optical Image: (a) Lidar Point Cloud, (b) Lidar Intensity Image, (c) Corresponding Optical Image; (d) Magnified Views of (a), (e) Magnified View of (b), and (f) Magnified View of (c).

Figure 1 shows one set of source data, including (1a) the lidar point cloud, (1b) the lidar intensity image, and (1c) the corresponding optical image. Figure 1d, 1e, and 1f demonstrate the details of (1a) the upper left image, (1b) the upper middle image, and (1c) the upper right image, respectively.

Linear and planar feature-based registration refers to registration of the optical images and lidar data using matching linear or planar features which exist in both optical images and lidar data. Schenk and Csathó (2002) proposed the sensor-invariant feature concept such as linear features and planar features for the registration of aerial imagery with lidar data for a more complete surface description. Roux *et al.* (2004) made use of the intrinsic rigidity of the aerial image to realize the registration of airborne lidar data with single aerial image, using planar features as Registration Primitives. Habib *et al.* (2004, 2005, and 2007) proposed the linear feature-based space resection and 3D to 3D transformation models for the registration of optical images and lidar data, and then also further combined these linear and planar features into a Multi-Primitive Triangulation Procedure for the integration of photogrammetry and lidar technology. Mitishita *et al.* (2008) completed the integration of photogrammetric and lidar data with the centroids of rectangular building roofs as control points in photogrammetric procedure. Wang and Neumann (2009) proposed a novel feature called 3CS to develop a robust automatic registration approach. Kyoungah *et al.* (2011) also proposed a method to simultaneously register images with lidar data, using area and linear primitives as ground control features. Linear and planar feature-based registration is mainly applied to areas rich in linear and planar features, such as buildings, roads, and urban areas, etc. However, this method causes difficulties in some other applications. For example, the data shown in Figure 1 have few distinct linear and planar features both in the optical image and lidar data, thus it is difficult to register the two data sources using linear

and planar feature-based registration. In addition, this method generally assumed that there is not a non-rigid deformation between the two data sources, thus camera calibration must be done before the optical image collecting. Otherwise, the non-rigid deformation caused by lens distortion cannot be eliminated.

As shown in Figure 1, it is difficult to process the source data with 2D image matching-based registration or linear and planar feature-based registration. First, the grayscale distribution of the lidar intensity image is very different from the optical image. Also, the lidar intensity image has low contrast and serious noise. Thus, neither point and line feature extraction nor the image matching is easy for data processing. Second, there are few planar features in the data set, and both the edge features in the optical image and the edge features in the lidar data are not always consistent with each other. These further lead to many difficulties in applying the linear and planar feature-based registration for the processing of the source data. Lastly, with limited distinction and smooth depth variation from one side to another, the linear and the planar features extracted from the lidar point cloud are not accurate enough to meet the requirements of the registration.

The principle of 3D to 3D point cloud-based registration is to transform the registration issue of 2D image with 3D lidar data into a 3D to 3D point cloud registration issue with computer vision or photogrammetric methods. Zhao *et al.* (2004) used stereo vision techniques to infer 3D structure from video sequences followed by 3D to 3D registration with the iterative closest point (ICP) algorithm. Pothoua and Karamitsos (2006) also developed two algorithms for the registration of optical image and lidar data, the principles of which were similar to the ICP algorithms and based on the minimization of the distances between points of one surface-to-surface patch of the other surface. Habib *et al.* (2006) improved the Hough Transform algorithm and the ICP algorithm, proposing

a registration method called MIHT/ICP for automatic surface matching of lidar data and Magnetic Resonance Imaging (MRI). 3D to 3D point cloud based registration aligns the optical images to lidar data with the 3D points generated by computer vision or photogrammetric methods rather than matching the optical image and the lidar intensity image directly. The disadvantage is that 3D to 3D point cloud based registration must ensure that there is not a non-rigid deformation in the 3D points generated from the images. In other words, in order to eliminate the effect of the lens distortion, camera calibration must be done before the optical image collection, or plenty of ground control points must be set up for a self-calibration bundle adjustment. This will lead to an increased cost and complexity of the registration, which does not benefit the extensive application of a non-metric camera.

In conclusion, due to the differences between visible and infrared spectrum and the lack of linear and planar features, the current registration methods cannot meet all the requirements of the applications, i.e., the registration of optical images with terrestrial lidar data for preservation of certain cultural relics. In addition, the current methods are generally under the hypothesis that there are no lens distortions so that the non-rigid deformation cannot be considered in the registration. Therefore, a novel method for the registration of optical images and terrestrial lidar data is proposed in this paper. Similar to 3D to 3D point cloud based registration, the proposed method is practiced by minimizing the distances from the photogrammetric matching points to terrestrial lidar data surface with the collinearity equation as the basic mathematical model. The advantages are that the proposed method can implement the registration without feature extraction and segmentation in the lidar data, and the non-rigid deformation caused by lens distortion can be eliminated by a bundle adjustment method similar to self-calibration, taking the distortion parameters as partial unknowns. Neither camera calibration nor a large number of control points for a self-calibration are required in the approach, thus the proposed method is much more flexible and convenient in application.

In the following sections, this paper will discuss the principle, mathematical model and solution of the proposed method followed by the implementation of the proposed method in detail, including image matching, free net bundle adjustment, estimation of the initial parameters, and accuracy assessment etc. Then, experiments are carried out to verify the performance of the proposed method followed by conclusions and future work.

Principle and Mathematical Model

Fundamental Principle

The fundamental principle of our method is clearly illustrated in Figure 2. In Figure 2a, the primary reference coordinate systems are shown, where C_1 and C_2 are the image space coordinate systems defined by the cameras, L is the sensor coordinate system defined by the terrestrial laser scanner, and W is the object space coordinate system. The point clouds captured by the laser scanner is normally located in the sensor coordinate system, L . In this paper, the registration of the optical images with the point cloud can be achieved without consideration of the object space coordinate system W . In other words, the 3D point P_0 can be assumed to locate in the sensor coordinate system L , and then the registration is equivalent to transforming the image space coordinate systems into the sensor coordinate system L by adjusting the parameters of the cameras and the images.

As shown in Figure 2b, an image captured by a digital camera is normally the central projection that transforms the real 3D scene into a 2D image, and the conjugate rays corresponding to the points in different images intersect in the same 3D points. Furthermore, a lidar point cloud can also be seen as the discrete samples of the continuous scene. Suppose several conjugate rays intersect in a 3D point $P(X, Y, Z)$, and this point will not necessarily fall on the lidar data surface. In other words, the distance from P to the lidar data surface signed as d is not zero. Therefore, the principle of the proposed method in this paper can be summarized as follows:

1. The 3D point P generated by photogrammetry should be as close to the lidar data surface as possible. This is called the Closest Point Principle.
2. The conjugate rays corresponding to different image points should intersect at the same 3D point P in the 3D scene, is the well-known forward intersection principle of photogrammetry.

The Closest Point Principle

Based on the discussion in *Fundamental Principle* subsection, suppose P is a 3D point generated by forward intersection, and the distance from P to the lidar data surface is d . Though P cannot be found with complete accuracy in the lidar point cloud, it is generally supposed to be on the lidar data surface, thus d should be possibly and infinitely close to zero. Suppose further that the real surface is smooth enough to be fitted by the normal plane locally, and the closest point of P in

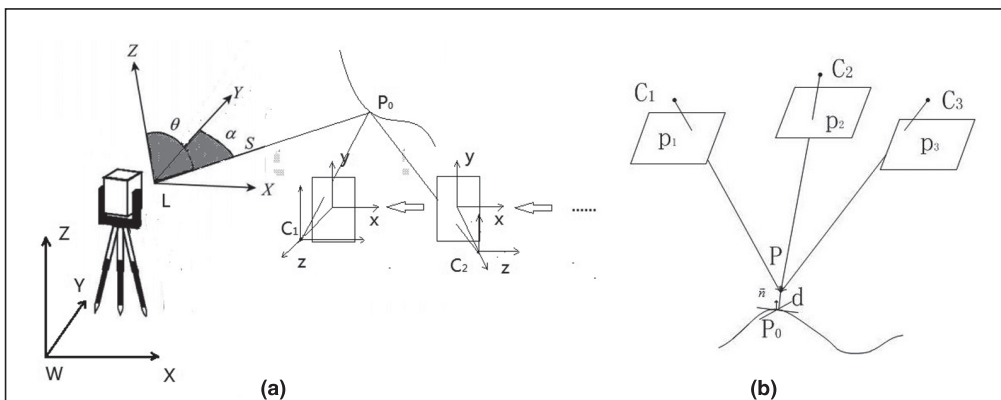


Figure 2. Fundamental Principle: (a) The Coordinate Systems, and (b) The Geometric Relationship between the Images and the Point Cloud.

the lidar point cloud and the corresponding normal vector are $P_0(X_0, Y_0, Z_0)$, and $\vec{n} = [n_x \ n_y \ n_z]^T$, respectively, then the equation of the normal plane at P_0 can be expressed as:

$$\vec{n} \bullet (P_x - P_0) = 0 \quad (1)$$

where P_x represents an arbitrary point on the normal plane.

And then the distance from P to the lidar data surface can be estimated by the following equation:

$$\tilde{d} = \vec{n} \bullet (P - P_0) \rightarrow 0. \quad (2)$$

The error equation corresponding to Equation 2 is acquired by first-order Taylor series expansion, which can be expressed as follows:

$$v_p = \vec{n}^T \Delta P - \vec{n} \bullet (P_0 - P^{(0)}) \quad (3)$$

where $\Delta P = (\Delta X \ \Delta Y \ \Delta Z)^T$ is the correction term of the coordinates of point P , and $P^{(0)}$ is the initial value of the coordinates of point P .

Finally, it should be noted that the normal vector at P_0 can be estimated by fitting a plane with several approximate points. In order to improve computational efficiency, this paper makes use of K-D tree (DeBerg *et al.*, 2000) for the searching of closest points, such as the closest point of P in the lidar data and the closest points around P_0 for the normal vector estimation.

Collinearity Equations

As discussed in the *Fundamental Principle* subsection, the 3D point P generated by forward intersection should meet the following collinearity equations (Mikhail and Bethel, 2001):

$$\begin{cases} x - x_0 - \Delta x = -f \frac{a_1(X - X_s) + b_1(Y - Y_s) + c_1(Z - Z_s)}{a_3(X - X_s) + b_3(Y - Y_s) + c_3(Z - Z_s)} \\ y - y_0 - \Delta y = -f \frac{a_2(X - X_s) + b_2(Y - Y_s) + c_2(Z - Z_s)}{a_3(X - X_s) + b_3(Y - Y_s) + c_3(Z - Z_s)} \end{cases} \quad (4)$$

where

$$\begin{cases} \Delta x = (x - x_0)(k_1 r^2 + k_2 r^4) + p_1[r^2 + 2(x - x_0)^2] \\ \quad + 2p_2(x - x_0)(y - y_0) \\ \Delta y = (y - y_0)(k_1 r^2 + k_2 r^4) + p_2[r^2 + 2(y - y_0)^2] \\ \quad + 2p_1(x - x_0)(y - y_0) \\ r = \sqrt{(x - x_0)^2 + (y - y_0)^2} \end{cases} \quad (5)$$

Similar to self-calibration (Mikhail and Bethel, 2001), error equations corresponding to the collinearity equations are illustrated by first-order Taylor series expansion and they can be expressed as follows:

$$V_{x,y} = A_{x,y} \Delta t + B_{x,y} \Delta P + C_{x,y} \Delta c + D_{x,y} \Delta k - L_{x,y} \quad (6)$$

where $V_{x,y} = [v_x \ v_y]^T$ is the residual vector of image point observation $(x \ y)^T$, and Δt , ΔP , Δc and Δk , respectively, stand for the correction terms of exterior orientation parameters, object point coordinates, principal point coordinates and the principal distance, and the lens distortion parameters. In addition, $A_{x,y}$, $B_{x,y}$, $C_{x,y}$, and $D_{x,y}$ refer to the first-order partial derivatives of error equations related to the correction terms above, $L_{x,y}$ the constant item calculated by the approximate values of unknowns.

Bundle Adjustment Model

According to the fundamental principle previously discussed, the interior and exterior parameters, and the coordinates of

the points generated by forward intersection should meet Equations 1 and 4 or the corresponding error Equations 3 and 6 at the same time. Therefore, to further consider the virtual observation equation of the interior parameters and the lens distortion parameters, the error equations of the proposed method can be written as follows:

$$\begin{cases} V = A \Delta t + B \Delta P + C \Delta c + D \Delta k - L & W \\ V_p = N \Delta P & -L_p \quad W_p \\ V_c = \Delta c & -L_c \quad W_c \\ V_k = \Delta k & -L_k \quad W_k \end{cases} \quad (7)$$

where V is the residual vector of observations consisting of $V_{x,y}$ in error Equation 6, V_p is the residual vector of observations consisting of v_p in error Equation 3; V_c and V_k are the error vectors of the virtual observation equations of the interior parameters and the lens distortion parameters. A , B , C , and D are the coefficient matrix which consists of all $A_{x,y}$, $B_{x,y}$, $C_{x,y}$, and $D_{x,y}$ in the collinearity error Equation 6, N is the coefficient matrix that consists of all the coefficients of the error Equation 3, L , L_p , L_c , and L_k are the corresponding constant items, and W , W_p , W_c , and W_k are the corresponding weight matrices.

Normal Equation Structure and Solution

The total normal equation with respect to the error Equation 7 is sparsely symmetric, but due to the introduction of plenty of 3D coordinates of the points generated by forward intersection, it is so large-scale that both the normal equation formation and solution are time-consuming. In other words, a fast algorithm for the normal equation formation and solution must be put forward to ensure the practical applicability of the proposed registration method. Fortunately, according to the form of the error Equation 7, the normal equation has a well-defined banded and bordered structure, as shown in Figure. 3. Therefore, in order to reduce the sizes of the normal equations, the reduced normal equations can be illustrated by eliminating the 3D point coordinate corrections, taking

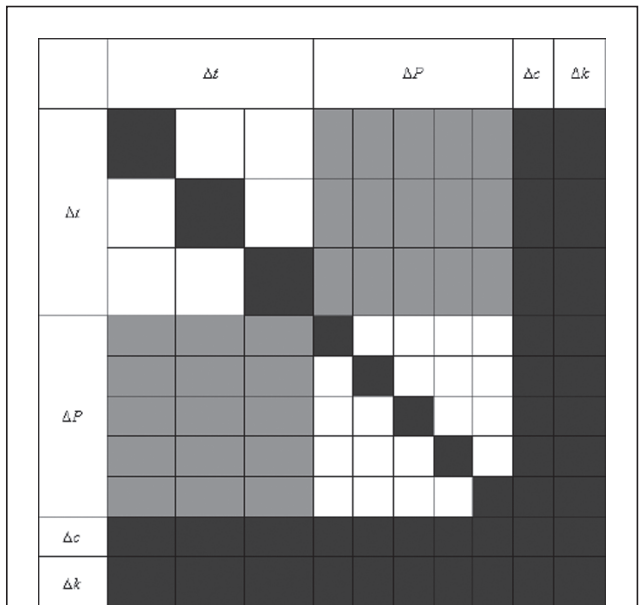


Figure 3. Normal Equation Structure.

advantage of the well-defined structure (Triggs *et al.*, 2000; Mikhail and Bethel, 2001). Furthermore, thanks to the powerful computer performance, solving the reduced normal equations with the Cholesky method has already met the requirements of the proposed registration method.

Figure 3 takes a data set consisting of three images and five 3D matching points as an example to illustrate the normal equation structure, where Δt , ΔP , Δc and Δk , present the positions of the corresponding corrections. The coefficient matrix is symmetric and positive, definite and sparse. The whites and the blacks are the zero and the non-zero blocks, respectively, while the possibility of the grays being zero is decided by whether the point occurs on the corresponding image or not.

Eliminate Influence of Gross Errors

There exist inevitable gross errors in image matching, and the measuring range of the images cannot always be the same as the lidar data. These factors may cause inaccuracy in the proposed registration method. Therefore, this paper sets up Gross Rate signed ε to restrain these unfavorable factors. The specific procedure is as follows: (a) The 3D points generated by forward intersection are firstly put in order according to the distances from the points to the lidar data surface; (b) Then, ε percent of the 3D points with the greatest distances are removed as gross errors; and (c) Finally, the registration is completed by using the proposed method with the remaining points.

Implementation

As previously mentioned, the implementation flow of the proposed registration method can be divided into two parts: preprocessing and registration, as shown in Figure 4. The preprocessing stage contains image matching, free net bundle adjustment and lidar data alignment. This paper focuses on the registration stage, which is further divided into three main parts: estimating the initial parameters, iterative calculations, and accuracy assessment.

Image Matching

As other applications of photogrammetry, image matching is also significant in the proposed procedure. The procedure

makes use of the matching points in the overlapping of the optical images to realize the registration of optical images with lidar data, thus accurate corresponding points must be matched properly to ensure the efficient and quality of the registration. Otherwise, the registration accuracy will decrease or even it will fail to execute the registration procedure.

Fortunately, a lot of research on image matching have already been done by the experts in the field of photogrammetry and computer vision so that the proposed registration procedure can employ these methods to accomplish the optical image matching, e.g., the approach proposed by Snavely *et al.* (2007) and the DPGGrid developed by Zhang *et al.* (2011). In detail, this paper is mainly focusing on the model, the procedure, and the solution of the registration, so the DPGGrid low altitude photogrammetry method (Zhang *et al.*, 2011) is used to generate the corresponding points of the optical images. Because the image matching of DPGGrid low altitude photogrammetry (Zhang *et al.*, 2011) is based on scale-invariant feature transform (SIFT) operator (Lowe, 2004) that are invariant to image scaling and rotation, and partially invariant to changes in illumination and 3D camera viewpoint, it is feasible and enough to meet the proposed registration procedure, as shown in Figure 5.

Free Net Bundle Adjustment

In order to implement the proposed registration method effectively, the exterior parameters of the images and the coordinates of the matching points are first estimated under an arbitrary coordinate system by free net bundle adjustment after the image matching. In this approach, the principal point is set as zero, and the principal distance is set as the focal length of the camera. The results contain the relative orientation parameters, the 3D object points and the corresponding image points. Figure 6 shows some results of the data preparation by using an arbitrary data set as an example, whereas Figure 6a presents the images arranged in order according to the connections in the strip, and Figure 6b presents the results of the free net bundle adjustment.

Alignment of Different Lidar Data

If the lidar point clouds are collected from different sites, they must be aligned to a common coordinate system before registration. In this paper, the alignment of different lidar data

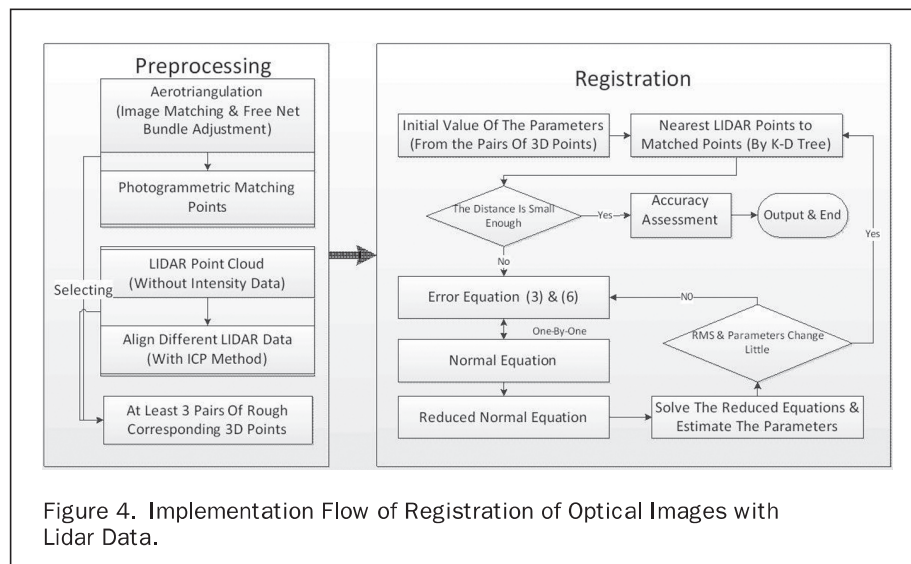


Figure 4. Implementation Flow of Registration of Optical Images with Lidar Data.



Figure 5. Image Matching of One Pair of Images.

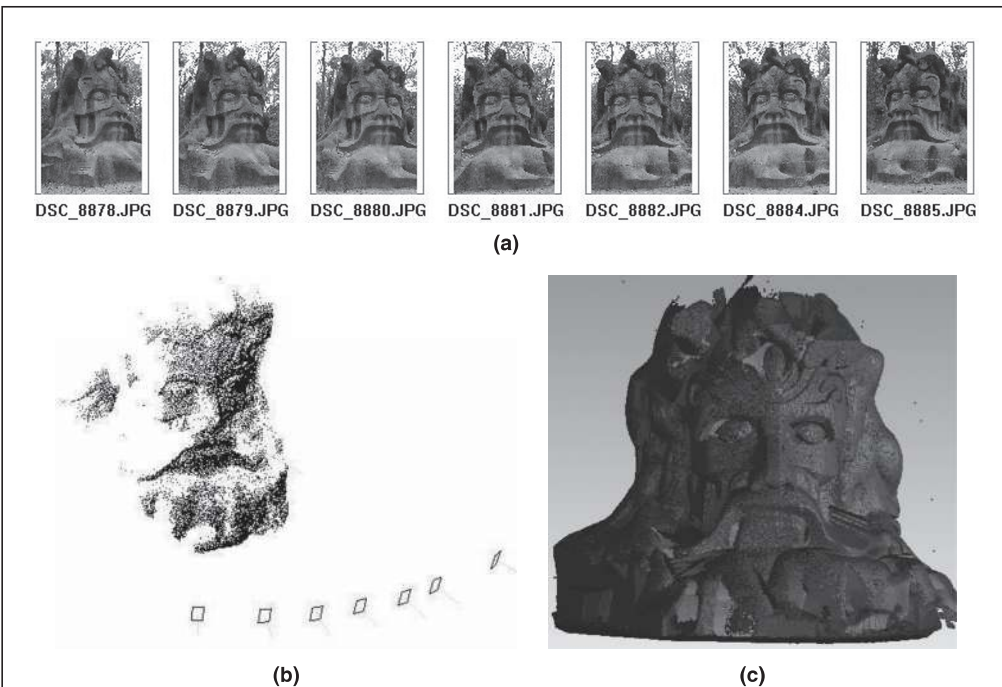


Figure 6. Data Preparation for Registration: (a) Arranged Optical Images, (b) Free Net Bundle Adjustment Result, and (c) Alignment of Different Lidar Data.

is done with the ICP algorithm proposed by Besl and McKay (1992). Figure 6c shows the alignment result of three different lidar point clouds, where different grays present the point clouds corresponding to different sites.

Estimation of Initial Values of the Parameters

To roughly estimate the image orientation parameters in the coordinate reference frame of the lidar data, the three-dimensional similarity transformation between the two data will be estimated after the completion of the free net bundle adjustment and the alignment of the lidar point clouds. This paper selects three pairs of coarse conjugate points between the free net bundle adjustment result and the lidar data, and the three-dimensional similarity transformation is then estimated by absolute orientation (Mikhail and Bethel, 2001).

Suppose the estimated three-dimensional similarity transformation can be expressed as follows:

$$X_{LiDAR} = sR_t X_{Photogrammetry} + T \quad (8)$$

where X_{LiDAR} and $X_{Photogrammetry}$ stand for the coordinates of lidar point and free net bundle adjustment point respectively, s is the scale factor, R_t the rotation matrix of the three-dimensional similarity transformation and T the translation vector.

The coordinates of the projection centers of the images can be estimated by using Equation 8 directly while the rotation matrices describing the attitudes of the images can be estimated as follows:

1. Transform the attitude parameters of any one of the optical images into corresponding rotation matrix and sign the rotation matrix as R .
2. Calculate the rotation matrix R' with Equation 9 as follows:

$$R' = R_t R. \quad (9)$$

3. Obtain three independent attitude angles from the rotation matrix R' . These attitude angles are relative to the coordinate frame of the lidar data, thus they can be used as the initial values for the registration of optical images and lidar data.

In addition, the initial values of the 3D points generated by forward intersection can be transformed into the coordinate reference frame by Equation 8 or by forward intersection with the previously mentioned initial exterior parameters.

Iterative Calculations and Accuracy Assessment

After the acquisition of the initial values of the parameters, the iterative calculations and accuracy assessment can be conducted according to the implementation flow shown in Figure 4 to complete the registration. The principle and the mathematical model of the registration have already been discussed in detail. In this section, the accuracy assessment methods in this paper are discussed first, and the procedure is then summarized.

As in any other least squares solution, the unit weighted root mean square (RMS) is used to evaluate the registration quality. According to error Equation 7, the unit weighted RMS can be expressed as follows:

$$RMS_0 = \sqrt{\frac{V^T WV + V_p^T W_p V_p + V_c^T W_c V_c + V_k^T W_k V_k}{n - r_t - r_p - r_c - r_k}}. \quad (10)$$

In this equation, n is the number of the observations, and r_t , r_p , r_c , and r_k are the numbers of exterior parameters, coordinates of the 3D points generated by forward intersection, interior parameters, and lens distortion parameters, respectively.

In addition, the RMS_i of the image point observations and the RMS_p of the distance observations of the photogrammetric

points are also employed to evaluate the registration quality. Their expressions are as follows:

$$RMS_i = \sqrt{\frac{V^T WV}{n_i}} \quad (11)$$

$$RMS_p = \sqrt{\frac{V_p^T W_p V_p}{n_p}} \quad (12)$$

Where n_i and n_p are the number of image point observations and the distance observations. Another accuracy assessment method in this paper is a statistics method called distance RMS (DRMS). When all the parameters are estimated after the registration, the 3D coordinates of the matching points can be calculated by using forward intersection, and then the distances from the 3D points to the lidar Data surface can be estimated by Equation 2 ($\tilde{d} = \tilde{n} \bullet (P - P_0) \rightarrow 0$). Finally, the DRMS can be estimated as follows:

$$DRMS = \sqrt{\frac{\sum \tilde{d}^2}{n_d}} \quad (13)$$

where n_d is the number of 3D points generated by photogrammetry.

To avoid accuracy underestimation caused by gross errors, the distances from the 3D points to the lidar data surface can be put in order, and then DRMS can be estimated by using only a certain percent of the smallest distances, i.e., 95 percent.

The last accuracy assessment method is to utilize Least Squares Image Matching (LSM). To evaluate the registration quality with LSM, several uniformly distributed checkpoints are firstly selected from the lidar data and then projected to the images. Then for each pair of the overlapping images, fix one of the projected image points, and search for the corresponding point using LSM with another projected image point as the initial matching point. Suppose the correction relative to the initial matching point is ΔD , the accuracy can be evaluated by using the following equation:

$$RMS_L = \sqrt{\frac{\sum \Delta D^2}{num}} \quad (14)$$

where num is the number of the image points matched by LSM. The procedure can now be as follows:

1. Find the closest point of the 3D points generated by forward intersection from the lidar data, and then fit a local plane to estimate the normal vector using the approximate lidar points. Next, estimate the DRMS and check if the DRMS is small enough to go to (4) for accuracy assessment. Otherwise, go to (2).
2. Construct error equations and normal equations, and then reduce structure parameters (the corrections of the coordinates of the 3D points) of the normal equations. Furthermore, solve the reduced normal equation to get the corrections of the interior and exterior parameters, and then obtain the corrections of the 3D coordinates with back-substitution. Finally, correct the parameters, calculate the unit weighted RMS and go to the next step.
3. Check the unit weighted RMS and the corrections of the parameters. If they are small enough, go to (1). Otherwise, go to (2).
4. The registration is finished and the quality is analyzed: calculate and output the unit weighted RMS, DRMS, and RMS_L for accuracy assessment.

Experiments and Results

Experimental Data

In order to test the performance of the proposed method, two different data sets are acquired by a laser scanning device and

non-metric cameras. The laser scanning device used in this paper is RIEGL VZ-400 with accuracy in the measurement range of 5 mm. The digital camera used in the acquisition of the optical images of data I is Nikon D300 with a focal length of about 28 mm. The size of the images is $4,288 \times 2,848$ pixels, and the pixel size is 0.0055 mm. The camera used to acquire the images of data II is a Cannon EOS 5D Mark II with a focal length of about 28 mm. The size of the images is $5,616 \times 3,744$ pixels, and the pixel size is 0.0064 mm. Neither the Nikon D300 nor the Cannon EOS 5D Mark II was calibrated before the registration.

Data I is a stone carving located in the foot of Bangmoshan, Wuhan, China, and data II in one cave of the Dazu Rock Carvings, Chongqing, China. More information about these data sets is shown in Table 1. Note that the matching point column presents the number of the 3D points generated by image matching.

The distribution of the above experimental images appears in Figure 7. As shown in the figure, the images of the left wall, the front wall and the right wall of data II are collected and processed, respectively. The numbers of the left wall and the right wall images are both 49 and uniformly distributed in seven strips, while the number of the front wall

TABLE 1. INFORMATION OF EXPERIMENTAL DATA

| Data | Images | Lidar sites | Strips | Matching Points | Other Information |
|------|--------|-------------|--------|-----------------|---|
| I | 7 | 3 | 1 | 24982 | Convergent photography, Shoot distance is 3 m. |
| II | 154 | 4 | 22 | 27061 | Normal case photography, Shoot distance is 1 m. |

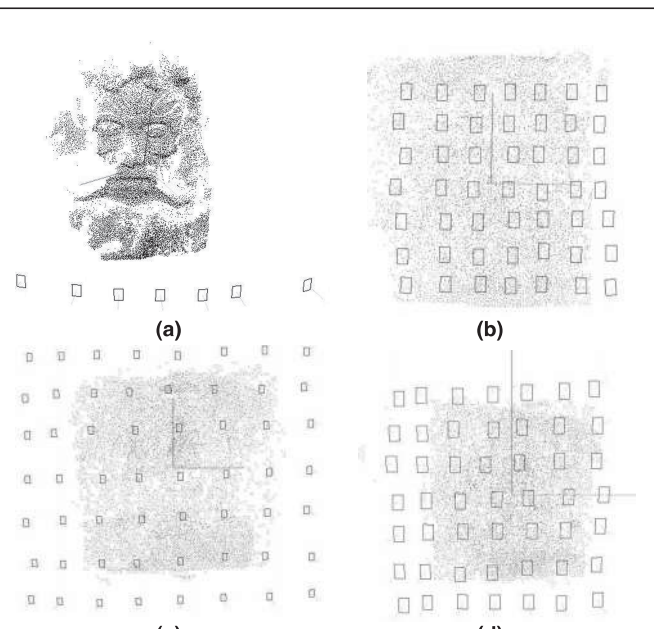


Figure 7. Distribution of Experimental Images: (a): Data I; (b) Left Wall, (c) Front Wall, and (d) Right Wall of Data II. The rectangles present the optical images, and the black points present the 3D points generated by photogrammetric image matching.

images is 56 and uniformly distributed in eight strips. In addition, the numbers of photogrammetric matching points of data II are 8,840, 9,194, and 9,027, respectively.

Both lidar point clouds of data I and data II are collected from multiple sites, thus the different point clouds should be aligned to a common coordinate reference frame before the registration. In the experiments, the alignment accuracy of the lidar point clouds is less than 5 mm.

Results of Unit Weighted RMS

The unit weighted RMS of the experiments is estimated by Equations 10, 11, and 12 after the registration, and the results are illustrated in Table 2.

Table 2 shows that the unit weighted RMS of the image point observations is less than 1 pixel and the unit weighted RMS of the distance observations is 3 mm to \sim 4 mm. In other words, the matching precision can reach a sub-pixel level. However, the unit weighted RMS of the distance observations can never be much less than 5 mm because the accuracy of the laser scanning device is 5 mm.

Results of DRMS

Table 3 shows the DRMS of the experiments where $DRMS_{0.95}$ represents the DRMS calculated by only using 95 percent of the smallest distances from the photogrammetric matching points to Terrestrial lidar data surface. The purpose of $DRMS_{0.95}$ is to avoid the unfavorable influence on the accuracy assessment caused by gross errors.

As indicated in Table 3, the DRMS of the data is far greater than $DRMS_{0.95}$. The reason is that there are a few gross errors in image matching. However, the fact that $DRMS_{0.95}$ reduces to less than 5 mm shows that most of the distances from photogrammetric matching points to the lidar data surface are rather small. Therefore, the proposed registration method in this paper can eliminate the influence of certain gross errors and offer high registration accuracy at the same time.

Results of LSM Accuracy Assessment

The accuracy assessment method with LSM previously provided is also used to evaluate the registration quality in these experiments. The results are shown in Table 4.

As can be seen in Table 4, the registration accuracies of data I and data II can both reach a sub-pixel level. Thus, the conclusion that the proposed registration method has a high accuracy is verified once again.

TABLE 2. RESULTS OF UNIT WEIGHTED RMS

| RMS | Data I | Data II | | |
|--------------|--------|---------|--------|--------|
| | | Left | Front | Right |
| RMS_0 | 0.0041 | 0.0034 | 0.0029 | 0.0032 |
| RMS_i (mm) | 0.0043 | 0.0033 | 0.0029 | 0.0032 |
| RMS_p (m) | 0.0029 | 0.0040 | 0.0037 | 0.0032 |

TABLE 3. RESULTS OF DRMS

| RMS | Data I | Data II | | |
|-------------------|--------|---------|--------|--------|
| | | Left | Front | Right |
| $DRMS$ (m) | 0.0153 | 0.0133 | 0.0028 | 0.1958 |
| $DRMS_{0.95}$ (m) | 0.0041 | 0.0012 | 0.0014 | 0.0013 |

Results of Interior and Lens Distortion Parameters

As in other normal least square adjustments, the theoretical accuracy of the unknown parameters can be estimated by the inverse coefficient matrix of the normal equations and the estimated unit weighted RMS. In this paper, we pay particular attention to the introduction of the interior and lens distortion parameters, thus the results of the interior and lens distortion parameters and their theoretical accuracies are illustrated in Table 5. The table shows that the interior and lens distortion parameters are significant in the experiments.

In addition, the significance of the introduction of the interior and lens distortion parameters can also be found by the follow fact: if the principal point and the lens distortion parameters are fixed to zeros and the principal distance is fixed to the focal length (28 mm), the registration accuracy decreases significantly, as shown in Table 6.

TABLE 4. STATISTICS OF REGISTRATION ACCURACY ESTIMATED BY USING LSM METHOD

| RMS | Data I | Data II | | |
|---------------------------|--------|---------|-------|-------|
| | | Left | Front | Right |
| RMS _x (pixel) | 0.71 | 0.46 | 0.46 | 0.46 |
| RMS _y (pixel) | 0.42 | 0.40 | 0.43 | 0.41 |
| RMS _{xy} (pixel) | 0.83 | 0.60 | 0.63 | 0.62 |

Texture Mapping Example

In this paper, the registration is mainly used to render the point clouds with texture for some cultural heritage conservation. So the image textures are also mapped onto the lidar data by using the estimated parameters, and the results are shown in Figure 8. The figure not only demonstrates that the estimated parameters can meet the requirements of data fusion and 3D reconstruction directly, but also verifies the effectiveness of the proposed method indirectly.

Conclusions and Future Work

We have proposed a novel method for registration of optical images with terrestrial lidar data. The method is implemented by minimizing the distances from the photogrammetric matching points to terrestrial lidar data surface with the collinearity equation as the basic mathematical model. The experiments show that the proposed method can be used to accurately and reliably implement the registration of optical images and lidar data, making it appropriate for data fusion and 3D reconstruction. In addition, with the introduction of lens distortion parameters, the non-rigid deformation caused by lens distortion can be effectively eliminated. Therefore, this proposed registration method is proved to be more convenient and flexible.

For these reasons, the proposed method is suitable for the registration of the optical images with the lidar data. However, if the lidar data surface is too flat, the proposed method will fail to work (or the normal equation becomes ill-conditioned). Therefore, the proposed method should be combined with other methods, i.e., the 2D image matching-based registration

TABLE 5. INTERIOR AND LENS DISTORTION PARAMETERS AND THEIR THEORETICAL ACCURACIES

| Item | Data I | | Data II | | | | | |
|------------|----------|----------|----------|----------|----------|----------|----------|----------|
| | Value | σ | Left | | Front | | Right | |
| | | | Value | σ | Value | σ | Value | σ |
| x_0 (mm) | -0.3348 | 0.0012 | 0.0456 | 0.00095 | -0.0331 | 0.00085 | -0.0107 | 0.00095 |
| y_0 (mm) | -0.0735 | 0.0011 | -0.0454 | 0.00095 | 0.0471 | 0.00086 | 0.1395 | 0.00096 |
| f(mm) | 28.5143 | 0.00016 | 28.2730 | 0.00014 | 28.6100 | 0.00012 | 28.2892 | 0.00014 |
| k_1 | -1.57e-4 | 8.9e-7 | -1.31e-4 | 1.9e-7 | -1.29e-4 | 1.8e-7 | -1.31e-4 | 2.0e-7 |
| k_2 | 2.44e-7 | 5.8e-9 | 1.54e-7 | 5.5e-10 | 1.56e-7 | 5.3e-10 | 1.54e-7 | 5.3e-10 |
| p_1 | -8.54e-5 | 1.9e-6 | -2.40e-6 | 1.5e-6 | 1.04e-5 | 1.4e-6 | -1.04e-5 | 1.3e-6 |
| p_2 | -1.74e-5 | 2.0e-6 | -8.89e-6 | 1.5e-6 | -9.29e-6 | 1.6e-6 | 1.73e-5 | 1.3e-6 |

TABLE 6. ACCURACY OF REGISTRATION (WITH FIXED INTERIOR AND LENS DISTORTION)

| Item | Data I | Data II | | |
|---------------------------------------|--------|---------|---------|--------|
| | | Left | Front | Right |
| RMS ₀ ^a | 0.0052 | 0.0070 | 0.0074 | 0.0066 |
| Increasing wrt Tab.2 ^b | 26.8% | 106.9% | 155.2% | 106.3% |
| DRMS _{0.95} ^c (m) | 0.0071 | 0.0138 | 0.0161 | 0.0124 |
| Increasing wrt Tab.3 ^d | 73.2% | 1050.0% | 1050.0% | 853.8% |

a, c: The meanings of RMS₀ and DRMS_{0.95} are the same as Table 2 and Table 3, respectively.

b: The increasing rate of RMS₀ with respect to Table 2.

d: The increasing rate of DRMS_{0.95} with respect to Table 3.

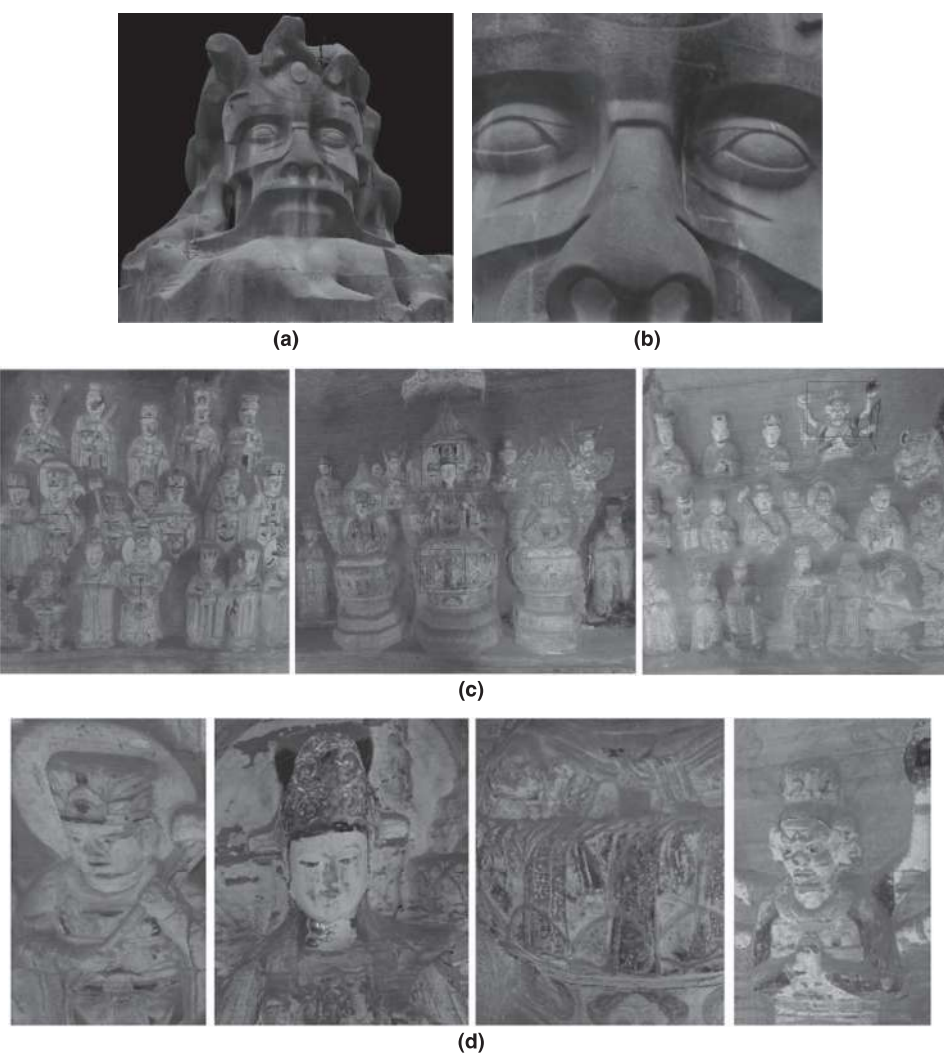


Figure 8. Texture Effects: (a): Texture Effect Of Data I; (b): Enlarged Detail of (a), (c): Left Wall, Front Wall, and Right Wall Texture Effects of Data II; and (d): Enlarged Details of (c).

and linear and planar feature-based registration, etc. Further studies are needed on the application of the proposed principle and mathematical model to the field of registration of aerial imagery with airborne lidar data.

Acknowledgments

This research is supported by the Chinese National Natural Science Foundation Program (No. 41071293; No. 41171357), the China's HuBei Province Natural Science Foundation Program (No. 2012FFB04202), and the Fundamental Research Funds for the Central Universities (No. 2012213020212; No. 201121302020005). We are very grateful to our colleagues, Professor Xiao Ma and Debra Leach for their precious comments and revision of the language, and special thanks are given to the anonymous reviewers and members of the editorial board for their suggestions of improving this article.

References

- Ackermann, F., 1999. Airborne laser scanning - Present status and future expectations, *ISPRS Journal of Photogrammetry and Remote Sensing*, 54(2-3):64–67.
- Baltsavias, E.P., 1999. A comparison between photogrammetry and laser scanning, *ISPRS Journal of Photogrammetry and Remote Sensing*, 54(2-3):83–94.
- Besl, P.J., and N.D. McKay, 1992. A method for registration of 3D shapes, *IEEE Transactions on Pattern Recognition and Machine Intelligence*, 14(2):239–256.
- Brown, L.G., 1992. A survey of image registration techniques, *ACM Computing Surveys*, 24:326–376.
- Cheng, L., J. Gong, M. Li, and Y. Liu, 2011. 3D Building model reconstruction from multi-view aerial imagery and lidar data, *Photogrammetric Engineering & Remote Sensing*, 77(2):125–139.
- DeBerg, M., O. Cheong, M. van Kreveld, M. Overmars, 2000. *Computational Geometry: Algorithms and Applications*, Second edition, New York: Springer.

- Ding, M., K. Lyngbaek, and A. Zakhor, 2008. Automatic registration of aerial imagery with untextured 3D LiDAR models, *Proceedings of the IEEE Conference on Computer Vision and Pattern Recognition*, pp.1–8.
- Habib, A.F., R.W.T. Cheng, E.-M. Kim, E.A. Mitishita, R. Frayne, and J.L. Ronsky, 2006. Automatic surface matching for the registration of LiDAR data and MR imagery, *ETR I Journal*, 28(2):162–174.
- Habib, A., M. Ghanma, M. Morgan, and R. Al-Ruzouq, 2005. Photogrammetric and lidar data registration using linear features, *Photogrammetric Engineering & Remote Sensing*, 71:699–707.
- Habib, A., M.S. Ghanma, C.J. Kim, and E. Mitishita, 2004. Alternative approaches for utilizing LiDAR data as a source of control information for photogrammetric models, *International Archives of Photogrammetry and Remote Sensing*, Vol.10, pp.1–6.
- Habib, A.F., K.I. Bang, and M. Aldelgawy, 2007. Integration of photogrammetric and lidar data in a multi-primitive triangulation procedure, *Proceedings of the ASPRS 2007 Annual Conference*, Tampa, Florida, 07-11 May, unpaginated CD-ROM.
- Kurz, T.H., S.J. Buckley., and J.A. Howell., 2011. Integration of panoramic hyperspectral imaging with terrestrial lidar data, *The Photogrammetric Record*, 26(134):212–228.
- Kyoungah, C., H. Juseok, and L. Impyeong, 2011. Precise geometric registration of aerial imagery and LiDAR data, *ETRI Journal*, 33(4):506–516.
- Leberl, F., A. Irschara, T. Pock, P. Meixner, M. Gruber, S. Scholz, and A. Wiechert, 2010. Point clouds: Lidar versus 3D vision, *Photogrammetric Engineering & Remote Sensing*, 76(10):1123–1134.
- Liu, J.-K., R. Li, and D. Sagar, 2009. Estimation of blufflines using topographic lidar data and orthoimages, *Photogrammetric Engineering & Remote Sensing*, 75(1):69–79.
- Lowe, D.G., 2004. Distinctive image features from scale-invariant keypoints, *International Journal of Computer Vision*, 60(2):91–110.
- Mikhail, E.M., and J.S. Bethel, 2001. *Introduction to Modern Photogrammetry*, New York: John Wiley & Sons Inc., 496 p.
- Mitishita, E., A. Habib, J. Centeno, A. Machado, J. Lay, and C. Wong, 2008. Photogrammetric and LiDAR data integration using the centroid of a rectangular roof as a control point, *The Photogrammetric Record*, 23(121):19–35.
- Postolov, Y., A. Krupnik, and K. McIntosh, 1999. Registration of airborne laser data to surfaces generated by photogrammetric means, *International Archives of Photogrammetry and Remote Sensing*, 32(3W14):95–99.
- Pothoua, A., S. Karamitsos, A. Georgopoulos, and I. Kotsis, 2006. Assessment and comparison of registration algorithms between aerial images and laser point clouds, *Proceedings of the ISPRS, Symposium: From Sensor to Imagery*, Commission 1, WGI/2, Part A, France.
- Roux, M., 2004. Registration of airborne laser data with one aerial image, *International Archives of Photogrammetry and Remote Sensing*, Vol. XXXV, pp. 1043–1048.
- Schenk, T., and B. Csatho, 2002. Fusion of LiDAR data and aerial imagery for a more complete surface description, *International Archives of Photogrammetry and Remote Sensing*, XXXIV/3A, pp. 310–317.
- Snavely, N., S.M. Seitz, and R. Szeliski, 2007. Modeling the world from internet photo collections, *International Journal of Computer Vision*, 80:189–210.
- Triggs, B., P. McLauchlan, R. Hartley, and A. Fitzgibbon, 2000. Bundle adjustment - A modern synthesis, *Proceedings of the International Workshop on Vision Algorithms*, ICCV '99, Springer-Verlag, pp. 298–372.
- Vosselman G, Kessel P, and B.G.H. Gorte, 2005, The utilization of airborne laser scanning for three-dimensional mapping, *International Journal of Applied Earth Observation and Geoinformation*, 6 (3-4):177–186.
- Wang, L., N. Zheng, and W. Chaoyang, 2012. A robust multisource image automatic registration system based on The SIFT descriptor, *International Journal of Remote Sensing*, 33(12):3850–3869.
- Wang, L., U. Neumann, and A. Robust, 2009. Approach for automatic registration of aerial images with untextured aerial LiDAR data, *Computer Vision and Pattern Recognition*, pp. 2623–2630.
- Wu, H., Y. Li, J. Li, and J. Gong, 2010. A two-step displacement correction algorithm for registration of lidar point clouds and aerial images without orientation parameters, *Photogrammetric Engineering & Remote Sensing*, 76(10):1135–1145.
- Zhao, W., D. Nister, and S. Hsu, 2005. Alignment of continuous video onto 3D point clouds, *IEEE Transactions on Pattern Analysis and Machine Intelligence*, 27(8):1305–1318.
- Zhang, J., Z. Zhang, T. Ke, Y. Zhang, and Y. Duan, 2011. Digital Photogrammetry GRID (DPGRID) and its application, *Proceedings of the ASPRS 2011 Annual Conference*, Milwaukee, Wisconsin, 01-05 May.

(Received 05 September 2012; accepted 22 March 2013; final version 07 April 2013)

2013 PE&RS Offprint & Extra Pages Order Form

This is the only opportunity available to order additional offset printing quality copies of your article. PE&RS does not go back on press after the issue's publication. Offprints are only shipped when ordered; they are not complimentary. However, all authors will receive one complimentary copy of the PE&RS issue containing their article. This form should be completed as soon as the initial proof is received, and should be returned with payment for offprints and page charges to the Production Manager as indicated below

Article Description:

Article Title: _____

Author(s): _____

Manuscript # _____

Please refer to the price chart and conditions on the back of this form in order to complete the table below.

| Quantity | Description | Amount |
|--------------|---|--------|
| | Offprints | |
| | Journal Covers (actual issue cover) | |
| | Extra Pages @125 per page (each page over 7 journal pages, reference "Instructions to Authors") | |
| | Electronic copy of article in PDF format @ \$2.00 per page | |
| | Shipping (applies to offprints and covers only (see price chart and conditions on back of this form.) | |
| Total | | |

Shipping/Contact Information:

Name: _____ Email: _____

Affiliation: _____

Street Address: _____

City: _____ State/Province: _____

Zip Code/Postal Code: _____ Country: _____

Phone: _____ Fax: _____

Method of Payment:

Accepted manuscripts with color images will not be released for publication until this form is received along with payment. Payments must be made in US dollars, drawn on a US bank, or appropriate credit card. Make checks payable to ASPRS. Keep a copy for your records.

Visa MasterCard Discover American Express Check (print PE&RS issue date & manuscript # on check)

Name on Credit Card: _____ Signature: _____

Account Number: _____ Expires (MO/YR): _____

Phone number for person above: _____ Email Address: _____

Do you need a receipt? Receipts will be emailed. Email Address: _____

SEND this form along with method of payment to:

Production Manager, ASPRS, 5410 Grosvenor Lane, Suite 210, Bethesda, MD 20814-2160
rkelley@asprs.org or 301-493-0208 (fax)

If you have questions, please contact me at 301-493-0290 x107

02/20/2013

Conditions:

Offprints are only shipped when ordered; they are not complimentary. However, all authors will receive one complimentary copy of the PE&RS issue containing their article. Offprint prices are based on the number of pages in an article. Orders are restricted to the quantities listed below. If offprints are not ordered prior to the issue's publication, reprints may be provided in multiples of 100 at the customer's expense. Shipping prices are based on weight and must be added to offprint and journal cover prices for an order to be processed. If overnight delivery is required, customers must provide an account code for the expense of the service (please indicate carrier and account number in the itemized table next to "Shipping").

Prices:

Please enter the price that corresponds to the quantity of offprints and/or covers being ordered on the front of this form.

| Offprints and Covers | 25 | 50 | 75 | 100* |
|---|--------------------------------|-------|-------|-------|
| Offprints (1 to 4 page article) | 9.00 | 15.00 | 21.00 | 27.00 |
| Offprints (5 to 8 page article) | 15.00 | 27.00 | 39.00 | 51.00 |
| Offprints (9 to 12 page article) | 21.00 | 39.00 | 57.00 | 75.00 |
| Offprints (13 to 16 page article) | 27.00 | 51.00 | 75.00 | 99.00 |
| Journal Covers | 15.00 | 25.00 | 35.00 | 45.00 |
| Cover Sponsor (Applies to Outside Front Cover image suppliers only) | 475.00 for 1000 covers and TOC | | | |

| Domestic (UPS Ground) | 25 | 50 | 75 | 100* | Canada (Air Parcel Post) | 25 | 50 | 75 | 100* |
|---|------------------------------------|-------|-------|-------|---|------------------------------------|-------|-------|-------|
| Offprints (1 to 4 page article) | 7.59 | 7.98 | 9.08 | 8.69 | Offprints (1 to 4 page article) | 19.14 | 20.78 | 21.45 | 22.11 |
| Offprints (5 to 8 page article) | 7.98 | 9.08 | 9.57 | 10.53 | Offprints (5 to 8 page article) | 20.68 | 22.11 | 23.87 | 25.74 |
| Offprints (9 to 12 page article) | 8.25 | 9.57 | 9.79 | 10.23 | Offprints (9 to 12 page article) | 21.45 | 23.87 | 26.57 | 28.82 |
| Offprints (13 to 16 page article) | 8.69 | 9.79 | 10.23 | 11.44 | Offprints (13 to 16 page article) | 22.11 | 25.74 | 28.85 | 31.96 |
| Journal Covers | 7.59 | 7.98 | 8.25 | 8.64 | Journal Covers | 19.14 | 20.68 | 21.45 | 22.11 |
| Cover Sponsor (Applies to Outside Front Cover image suppliers only) | 70.00 | | | | Cover Sponsor (Applies to Outside Front Cover image suppliers only) | Contact ASPRS for Shipping Prices. | | | |
| Mexico (Air Parcel Post) | 25 | 50 | 75 | 100* | Overseas (Air Parcel Post) | 25 | 50 | 75 | 100* |
| Offprints (1 to 4 page article) | 22.39 | 23.87 | 24.75 | 27.12 | Offprints (1 to 4 page article) | 28.05 | 30.31 | 41.69 | 36.06 |
| Offprints (5 to 8 page article) | 24.11 | 27.12 | 30.64 | 34.50 | Offprints (5 to 8 page article) | 30.36 | 36.03 | 45.26 | 47.41 |
| Offprints (9 to 12 page article) | 25.52 | 30.69 | 36.03 | 40.26 | Offprints (9 to 12 page article) | 33.17 | 41.69 | 49.55 | 55.99 |
| Offprints (13 to 16 page article) | 27.12 | 34.60 | 40.26 | 45.98 | Offprints (13 to 16 page article) | 36.03 | 47.41 | 55.99 | 64.51 |
| Journal Covers | 22.33 | 23.87 | 25.52 | 27.12 | Journal Covers | 28.05 | 30.31 | 41.69 | 46.03 |
| Cover Sponsor (Applies to Outside Front Cover image suppliers only) | Contact ASPRS for Shipping Prices. | | | | Cover Sponsor (Applies to Outside Front Cover image suppliers only) | Contact ASPRS for Shipping Prices. | | | |

Assignment of Copyright to ASPRS

Current copyright law requires that authors of papers submitted for publication in *Photogrammetric Engineering & Remote Sensing* transfer copyright ownership to the American Society for Photogrammetry and Remote Sensing before the paper may be published. Upon receipt of this form with your Master Proof, please complete this form and forward it to the Production Coordinator (address below).

Manuscript Title: _____

Author(s): _____

Assignment of Copyright in the above-titled work is made on (date) _____ from the above listed author(s) to the American Society for Photogrammetry and Remote Sensing, publisher of *Photogrammetric Engineering & Remote Sensing*.

In consideration of the Publisher's acceptance of the above work for publication, the author or co-author(s) hereby transfer(s) to the American Society for Photogrammetry and Remote Sensing the full and exclusive copyright to the work for all purposes for the duration of the copyright. I (we) understand that such transfer of copyright does not preclude specific personal use, provided that prior to said use, permission is requested from and granted by the American Society for Photogrammetry and Remote Sensing.

I (we) acknowledge that this paper has not been previously published, nor is it currently being considered for publication by any other organization.

Author/co-author signatures

Co-authors may fill out and submit this form separately (photocopies are acceptable) if desired; but all co-authors must sign either this or a separate form.

Special Note to U.S. Government Employees

Material prepared by U.S. Government employees as part of their official duties need not have the assignment of copyright transferred since such material is automatically considered as part of the public domain.

If your paper falls within this category please check the appropriate statement and sign below.

This paper has been prepared wholly as part of my (our) official duties as (a) U.S. Government Employee(s). I (we) acknowledge that this paper has not previously been published, nor is it currently being considered for publication, by any other organization.

This paper has been prepared partly in the course of my (our) official duties as (a) U.S. Government Employee(s). For any part(s) not prepared in the course of my (our) official duties, copyright is hereby transferred to the American Society for Photogrammetry and Remote Sensing. I (we) acknowledge that this paper has not previously been published, nor is it currently being considered for publication, by any other organization.

Author/co-author signatures

Please return this form to:
Production Coordinator, ASPRS
5410 Grosvenor Lane, Suite 210
Bethesda, MD 20814-2160
301-493-0290, 301-493-0208 (fax), www.asprs.org

2013 PE&RS Color Order Form

Accepted manuscripts will not be released for publication until all color charges have been paid. Color payment should be made when final manuscript is accepted by the Editor-in-Chief. Payment and this form must be mailed/faxed to the ASPRS Production Manager at the address below.

Article Description:

Article Title: _____

Author(s): _____

Manuscript # _____

Color Plate Prices*

| 1 | 2 | 3 | 4 | 5 | 6 | 7 | 8 |
|--------------|---------|---------|---------|---------|---------|---------|---------|
| \$1000 | \$1,650 | \$2,225 | \$2,800 | \$3,375 | \$3,950 | \$4,525 | \$5,100 |
| Total | | | | | | | |

* For purposes of this form, a color plate is considered to be a plate that is numbered, even if it contains several parts, e.g. (a), (b), and so on.

Name/Contact Information of Author Submitting this Form:

Name: _____ Email: _____

Affiliation: _____

Address: _____

Phone: _____ Fax: _____

Method of Payment:

Accepted manuscripts with color images will not be released for publication until this form is received along with payment. Payments must be made in US dollars, drawn on a US bank, or appropriate credit card. Make checks payable to ASPRS. Keep a copy for your records.

Visa MasterCard Discover American Express Check (print PE&RS issue date & manuscript # on check)

Name on Credit Card: _____ Signature: _____

Account Number: _____ Expires (MO/YR): _____

Phone number for person above: _____ Email Address: _____

Do you need a receipt? Receipts will be emailed. Email Address: _____

SEND this form along with method of payment to:

Production Manager, ASPRS, 5410 Grosvenor Lane, Suite 210, Bethesda, MD 20814-2160
rkelley@asprs.org or 301-493-0208 (fax)

If you have questions, please contact me at 301-493-0290 x107

02/20/2013